J. Fluid Mech. (2008), *vol.* 599, *pp.* 465–476.
doi:10.1017/S0022112008000219 Printed in the United Kingdom

Steady-state solidification of aqueous ammonium chloride

S. S. L. PEPPIN†, HERBERT E. HUPPERT AND M. GRAE WORSTER

Institute of Theoretical Geophysics, Department of Applied Mathematics and Theoretical Physics, University of Cambridge, Wilberforce Road, Cambridge CB3 0WA, UK

(Received 10 July 2007 and in revised form 16 December 2007)

We report on a series of experiments in which a Hele-Shaw cell containing aqueous solutions of NH_4Cl was translated at prescribed rates through a steady temperature gradient. The salt formed the primary solid phase of a mushy layer as the solution solidified, with the salt-depleted residual fluid driving buoyancy-driven convection and the development of chimneys in the mushy layer. Depending on the operating conditions, several morphological transitions occurred. A regime diagram is presented quantifying these transitions as a function of freezing rate and the initial concentration of the solution. In general, for a given concentration, increasing the freezing rate caused the steady-state system to change from a convecting mushy layer with chimneys to a non-convecting mushy layer below a relatively quiescent liquid, and then to a much thinner mushy layer separated from the liquid by a region of active secondary nucleation. At higher initial concentrations the second of these states did not occur. At lower concentrations, but still above the eutectic, the mushy layer disappeared. A simple mathematical model of the system is developed which compares well with the experimental measurements of the intermediate, non-convecting state and serves as a benchmark against which to understand some of the effects of convection. Movies are available with the online version of the paper.

1. Introduction

Unidirectional solidification is an important processing technique for the fabrication of single-crystal superalloys. These materials are used, for example, to produce turbine blades that are resistant to creep and mechanical failure under the extremely demanding conditions found in modern turbojet engines. In directional solidification, the melt is pulled through a constant temperature gradient, with the bottom heat exchanger held below the eutectic temperature of the alloy. In carefully designed systems an entire turbine blade can be made with a single crystal forming the primary phase (Kear 1986).

At very low solidification rates melts doped with small amounts of impurity can solidify with a planar crystal–melt interface. However, even at quite modest rates of solidification, the crystal–melt interface deforms and protrudes into the melt owing to a morphological instability (Mullins & Sekerka 1964; Davis 2001). The melt is then separated from the solid by a mixed-phase region containing dendrites and interdendritic liquid, referred to as a mushy layer (Worster 2000). Buoyancy-driven convection can occur within the mushy layer as well as the melt, and can greatly

† Present address: Department of Geology and Geophysics, Yale University, New Haven, CT 06520-8109, USA.

affect the properties of the resultant solid (Huppert 1990; Huppert *et al.* 1993). Two significant defects related to convection are: freckling, i.e. long trails of segregated material appearing in the solid; and secondary nucleation of crystals in the melt, yielding a solid with internal grain boundaries along which creep can occur (Kurz & Fisher 1989).

In order to understand the origin of freckles, McDonald & Hunt (1970) and Copley *et al.* (1970) performed experiments on aqueous solutions of ammonium chloride (NH_4Cl), a system with similar physical properties to metallic alloys (Jackson *et al.* 1966), but having the advantages of transparency and low operating temperatures. By cooling the solution from a fixed chill, they discovered that freckles are the result of solvent-rich plumes emanating from dendrite-free channels, or 'chimneys' in the mushy layer.

A great deal of work has since been conducted on understanding the nature of chimneys and conditions under which they form (Roberts & Loper 1983; Fowler 1985; Worster 1991, 1992; Schulze & Worster 1999; Loper & Roberts 2001; Chung & Worster 2002). Most experimental work has involved cooling the solution from a fixed chill (Huppert & Worster 1985; Chen & Chen 1991; Tait, Jahrling & Jaupart 1992; Huppert & Hallworth 1993; Chen 1995; Wettlaufer, Worster & Huppert 1997; Solomon & Hartley 1998; Aussillous *et al.* 2006). Recently we have developed a new experimental apparatus in which the solution can be translated at prescribed rates through a fixed temperature gradient (Peppin *et al.* 2007). This configuration has the advantages of similarity to industrial solidification techniques and simplified steady-state mathematical analysis. In experiments on aqueous NaCl solutions in a non-convecting configuration we found that the mushy layer equations (Worster 2000) gave very accurate predictions of the mushy layer heights and measured temperature profiles.

In the present experiments we solidify aqueous NH_4Cl solutions in which buoyancy-driven convection gives rise to the formation of chimneys. We discover several different solidification regimes depending on the freezing velocity and concentration of the original solution. We also present and solve a simple model of the solidification process, which accounts for convection and undercooling at the mush–solution interface. In § 2 we briefly describe the apparatus and discuss the experimental protocol. Section 3 presents the main results of the experiments in the form of a regime diagram, with several representative movies illustrating the transitions in the diagram. The mathematical model is presented in § 4 and its predictions are compared with the measured temperature profiles and steady-state mushy layer thicknesses as functions of the freezing velocity. A discussion and summary of the results are given in §§ 5 and 6.

2. Experimental protocol

The experimental apparatus consists of a Hele-Shaw cell of internal dimensions $38 \times 12 \times 0.5\,\mathrm{cm}$ and made of Pyrex glass. The cell was translated at fixed rates between two sets of heat exchangers separated vertically by 6 cm. A schematic diagram of the system is given in figure 1. A more detailed description of the apparatus is given in Peppin *et al.* (2007). The fluids entering the upper and lower heat exchangers were cooled to $-35\,^{\circ}\mathrm{C}$ and $20\,^{\circ}\mathrm{C}$, respectively, yielding a temperature gradient of approximately $1\,^{\circ}\mathrm{C\,mm^{-1}}$. Experiments were performed on aqueous solutions of ammonium chloride with concentrations ranging between 21 and 27 wt %. The freezing velocities used ranged between 0.1 and $17\,\mu\mathrm{m\,s^{-1}}$. An

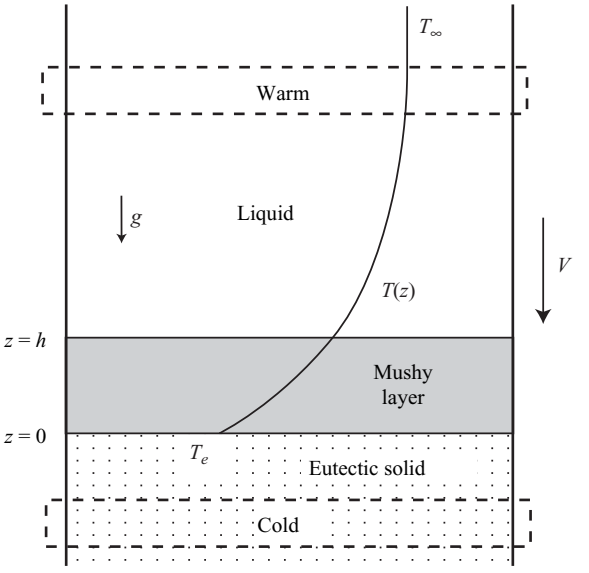

FIGURE 1. Schematic diagram of the solidification process showing a representative temperature profile. Gravity acts in the $-z$ direction. During an experiment the cell is pulled downward through the stationary heat exchangers (dashed lines) at constant speed V. The system is steady in a frame of reference fixed with respect to the heat exchangers.

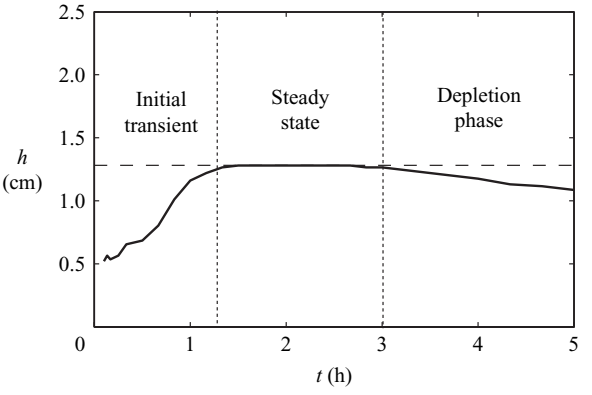

FIGURE 2. Height h of the mushy layer as a function of time t during an experiment using 25 wt% NH_4Cl with the cell translated at 3 μm s^{-1}. An initial transient period occurred during which the temperature profile stabilized and the mushy layer grew to a maximum height. The height remained constant for approximately 1.5 h, after which the bulk solution became depleted and h began to decrease. At very early times h was difficult to measure and is not shown.

experiment was initiated by pumping the coolant through the heat exchangers and simultaneously translating the cell at a fixed speed. Temperatures were recorded by an array of thermistors embedded in the side of the cell and, in some experiments, a single thermistor placed centrally in the cell. The steady-state height was taken to be the maximum height reached by the mushy layer during the course of an experiment (figure 2). At the lower concentrations less convection occurred and steady states lasting several hours could be achieved, similar to the experiments on NaCl (Peppin *et al.* 2007). At the highest concentration studied (27 wt %) convection in the mushy

layer and in the bulk solution was very strong and depletion of the bulk solution occurred, making it difficult to achieve long periods of a steady state.

3. Experiments on aqueous ammonium chloride

Depending on the initial solute concentration and freezing conditions a range of characteristic behaviours occurred. At low solidification rates and high concentration, the mushy layer tended to be thick and the mushy-layer Rayleigh number (Worster 1992) was relatively large, leading to convection in the layer and the formation of chimneys. Figure 3(*a*) is an image taken from an experiment using 23 wt % NH_4Cl with a pulling speed V of $0.5\,\mu m\,s^{-1}$; chimneys with associated plumes in the melt can be seen. Upon increasing the pulling speed to $2\,\mu m\,s^{-1}$ the chimneys were completely extinguished (figure 3*b*). This chimney to no-chimney transition is illustrated in movie 1. It was not possible to increase the pulling speed indefinitely, however, without eventually destroying the columnar nature of the mushy layer. At sufficiently high V the mushy layer would collapse to a smaller thickness, often with growth of new crystals in the vigorously convecting supercooled melt. At higher initial solution concentrations, the collapse of the mushy layer occurred even before the chimney to no-chimney transition (figure 3*c* and movie 2).

Our main experimental results are summarized in figure 4, which is a regime diagram for the solidification of aqueous NH_4Cl in a temperature gradient of approximately $1\,^{\circ}C\,mm^{-1}$ at the mush–liquid interface. The various symbols in the diagram correspond to different solidification regimes. The triangles represent experiments where chimneys were present at steady state. The chimneys could be extinguished by adjusting the freezing velocity. At intermediate concentrations (22 and 23 wt %) columnar mushy layers with no chimneys (stars in figure 4) could be produced for a range of velocities. At higher concentrations (25 and 27 wt %) the mushy layer with chimneys gave way to a regime of active growth of equiaxed crystals (crosses in figure 4) as the freezing velocity was increased. Some of these secondary crystals were clearly ejected from the mushy layer, and either melted in the warmer fluid or sedimented downward to re-enter the mush, while others appeared to nucleate and grow on the Pyrex sides of the Hele-Shaw cell. At the lowest concentration studied (21 wt %) we did not observe any chimneys even at the slowest freezing rate ($0.1\,\mu m\,s^{-1}$). Furthermore, no secondary crystals were observed, but instead at high V ($\geqslant 1\,\mu m\,s^{-1}$) the mushy layer completely disappeared, leaving only a composite eutectic growing below a highly supercooled melt (circles in figure 4; also see figure 3*d* and movie 3). This transition occurred also in the 22 wt % case ($V \geqslant 10\,\mu m\,s^{-1}$), and would presumably occur for even higher concentrations given sufficiently large pulling speeds.

From these observations we conclude that, in an NH_4Cl–H_2O system having a temperature gradient of $1\,^{\circ}C\,mm^{-1}$, if the bulk concentration is 25 wt% or higher then either there is a mushy layer with chimneys or there is nucleation and growth of secondary crystals. Only by reducing the bulk concentration does the possibility of growing a defect-free solid occur.

4. Mathematical modelling

We consider the case where there is convection in the melt, but no large-scale convection in the mushy layer (figure 3*b* and the * regime in figure 4). We neglect depletion of the bulk solution and assume that the concentration in the melt is

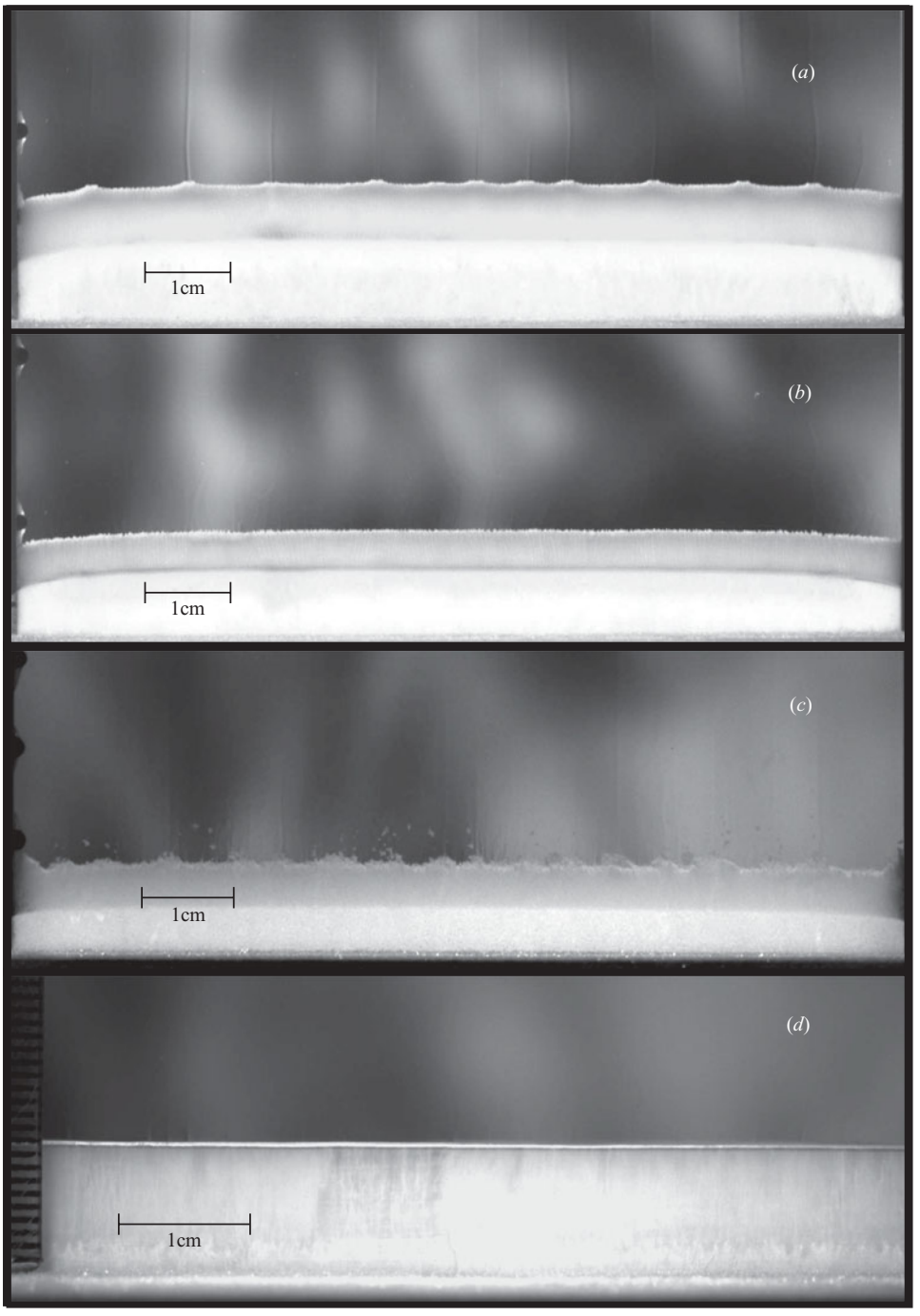

FIGURE 3. Steady-state solidification of NH_4Cl under various operating conditions. Image (*a*) shows a 23 wt % solution with the cell translated at 0.5 μm s^{-1}. The bright white solid at the bottom is the eutectic, above which is the mushy layer. Chimneys formed with associated plumes in the melt. In (*b*) the pulling speed was increased to 2 μm s^{-1} and the chimneys disappeared. Image (*c*) illustrates the growth of secondary crystals above the mushy layer in a 25 wt % solution translated at 6 μm s^{-1}. In (*d*) a 21 wt % solution was translated at 1 μm s^{-1} and no mushy layer formed above the composite eutectic solid.

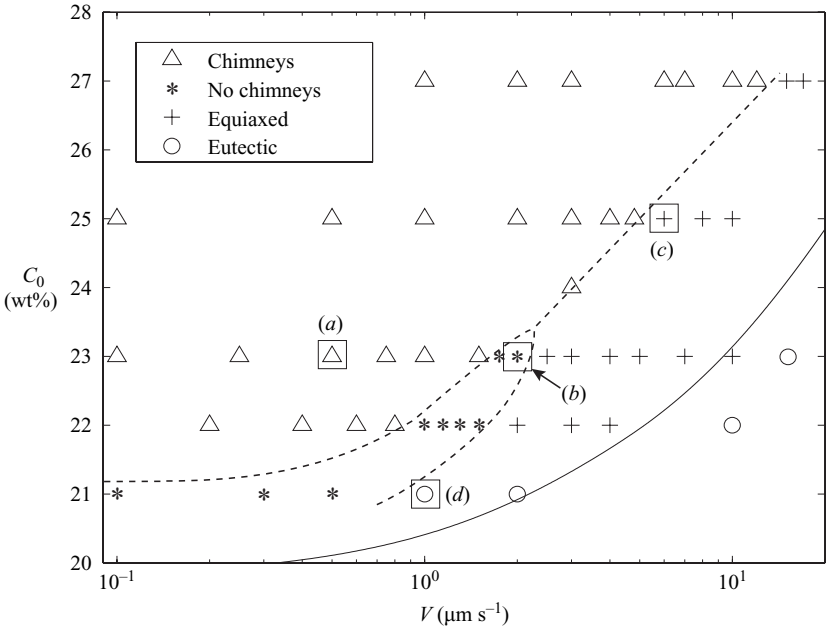

FIGURE 4. Regime diagram depicting the morphological transitions observed. Depending on the initial solution concentration C_0 and pulling speed V, four qualitatively different regimes occurred: a columnar mushy layer with chimneys (△), a columnar mushy layer with no chimneys (*), a collapsed mushy layer with growth of new crystals (+), and a eutectic with no mushy layer (○). The four data points enclosed by squares correspond to the four experiments depicted in figure 3. The dashed curves have been hand-drawn to aid visualization of the different regimes. The solid curve is the prediction of the disappearance of the mushy layer by the model developed in § 4.

constant and equal to the initial concentration C_0. Furthermore, we assume that convection in the melt is sufficiently slow that heat transfer occurs mainly by conduction. Theoretical support for this assumption comes from Emms & Fowler (1994), who showed that for laminar double-diffusive convection emanating from the mushy layer (such as is observed before the onset of chimneys) the temperature profile in the liquid is only slightly perturbed from a purely diffusive profile. The steady-state temperature profile in the melt is then given by

$$T(z) = T_\infty + [T(h) - T_\infty]\frac{\mathrm{e}^{r_1(z-L)} - \mathrm{e}^{r_2(z-L)}}{\mathrm{e}^{r_1(h-L)} - \mathrm{e}^{r_2(h-L)}}, \qquad h \leqslant z \leqslant L \tag{4.1}$$

(Peppin *et al.* 2007) where $T_\infty = 20\,^\circ\mathrm{C}$ is the temperature of the air surrounding the Hele-Shaw cell, $T(h)$ is the temperature at the interface between the mushy layer and melt, h is the thickness of the mushy layer, L is the position of the upper heat exchanger and $r_{1,2} = -\frac{1}{2}\mathscr{V} \pm \frac{1}{2}(\mathscr{V}^2 + 4b/k_l)^{1/2}$. Here $\mathscr{V} = Vc_l/k_l$, V is the speed of the cell, b is a coefficient accounting for heat transfer from the surroundings to the Hele-Shaw cell, and k_l and c_l are the effective thermal conductivity and volumetric heat capacity of the melt, defined as areal averages of those of the solution and the Pyrex sides of the Hele-Shaw cell by

$$k_l = \zeta k_{sol} + (1-\zeta)k_p, \qquad c_l = \zeta c_{sol} + (1-\zeta)c_p, \tag{4.2}$$

where $\zeta = 5/9$ is the fraction of the cross-sectional area of the Hele-Shaw cell occupied by the melt, $1-\zeta$ is the fraction occupied by the Pyrex glass, k is thermal conductivity, c is heat capacity per unit volume, and the subscripts '*sol*' and 'p' denote properties of the solution and Pyrex, respectively. Peppin *et al.* (2007) performed thermal characterization experiments to determine that the heat-transfer coefficient $b = 1.6 \times 10^3\ \mathrm{J\,m^{-3}\,s^{-1}\,K^{-1}}$.

Neglecting solute diffusion, we write conservation of energy and mass in the mushy layer as

$$-c_l V \frac{\mathrm{d}T}{\mathrm{d}z} = \frac{\mathrm{d}}{\mathrm{d}z} k_e \frac{\mathrm{d}T}{\mathrm{d}z} - \zeta \mathscr{L}_s V \frac{\mathrm{d}\phi}{\mathrm{d}z} - b(T - T_\infty), \qquad 0 \leqslant z \leqslant h, \tag{4.3}$$

$$(1-\phi)\frac{\mathrm{d}C}{\mathrm{d}z} = (C - C_s)\frac{\mathrm{d}\phi}{\mathrm{d}z}, \qquad 0 \leqslant z \leqslant h, \tag{4.4}$$

where ϕ is the volume fraction of NH_4Cl crystals in the mushy layer, $\mathscr{L}_s$ is the heat of solution per unit volume of solid, $C_s = 1$ is the mass fraction of NH_4Cl in the solid dendrites and C is the mass fraction of NH_4Cl in the interstitial liquid. This is related to T by the local equilibrium condition

$$T(z) = T_L(z) = T_e + \Gamma[C(z) - C_e], \qquad 0 \leqslant z \leqslant h, \tag{4.5}$$

where T_L is the liquidus temperature, T_e and C_e are the eutectic temperature and concentration, respectively, and Γ is the slope of the liquidus curve. The effective thermal conductivity is given by the expression $k_e = \zeta k_m + (1-\zeta)k_p$, where $k_m = \phi k_s + (1-\phi)k_{sol}$ is the thermal conductivity of the mushy layer and k_s is the thermal conductivity of pure NH_4Cl.

With the neglect of convection in the mushy layer (no chimneys) and the neglect of solute diffusion, the model has no flux of solute across the mush–liquid interface, in which case (4.4) implies that $(1-\phi)(C - C_s) = C_0 - C_s$, where C_0 is the bulk solution concentration. Inserting this result and (4.5) into (4.3), we obtain

$$\frac{\mathrm{d}}{\mathrm{d}z} k_e \frac{\mathrm{d}T}{\mathrm{d}z} = \left(\zeta \mathscr{L}_s \frac{[T_L(C_0) - T_L(C_s)]}{[T - T_L(C_s)]^2} - c_{le} \right) V \frac{\mathrm{d}T}{\mathrm{d}z} + b(T - T_\infty), \qquad 0 \leqslant z \leqslant h, \tag{4.6}$$

as the equation governing the temperature field in the mushy layer. Equation (4.6) is subject to the boundary conditions (Worster 1991)

$$T(0) = T_e, \qquad k_e \frac{\mathrm{d}T}{\mathrm{d}z}\bigg|_{h^-} = \zeta \mathscr{L}_s \phi(h) V + k_l \frac{\mathrm{d}T}{\mathrm{d}z}\bigg|_{h^+}, \tag{4.7}$$

where $\phi(h) = [T(h) - T_L(C_0)]/[T(h) - T_L(C_s)]$ and $T_z(h^+)$ is obtained from (4.1). The $z = 0$ position is taken to be the height at which the thermistor reading was equal to T_e.

In order to close the system of equations an additional boundary condition at $z = h$ is required. Following Worster & Kerr (1994), we account for convection in the melt by adopting an empirical undercooling condition at the mush–melt interface. We recognize, however, that in a complete theory the interfacial undercooling would be predicted as part of the solution. Potentially, such a theory might be developed by taking proper account of the double-diffusive layer in the melt. We measured the interfacial undercooling for experiments with no chimneys or weak chimneys (figure 5) and fitted the data to a second-order polynomial of the form

$$V = G_1[T_L(C_0) - T(h)] + G_2[T_L(C_0) - T(h)]^2, \tag{4.8}$$

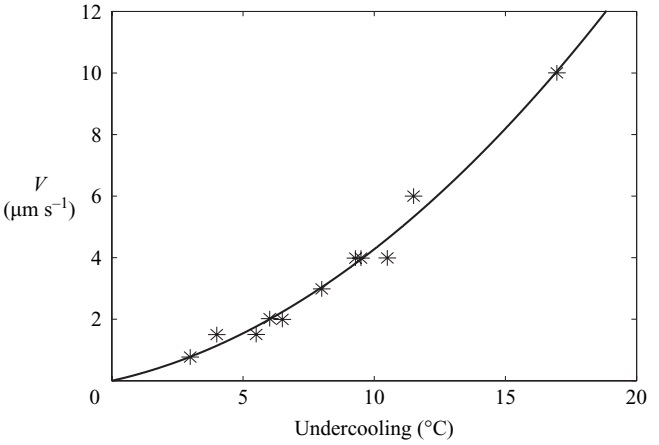

FIGURE 5. Measured undercooling (below the bulk freezing temperature) of the interface between the mushy layer and the solution as a function of the pulling speed V. The solid curve is a least-squares fit of the data to a second-order polynomial.

Symbol	Value	Symbol	Value	Symbol	Value
k_{sol}	$0.54\,\mathrm{J\,m^{-1}\,s^{-1}\,K^{-1}}$	ρ_{sol}	$1050\,\mathrm{kg\,m^{-3}}$	c_{sol}	$3.68\times10^{6}\,\mathrm{J\,m^{-3}\,K^{-1}}$
k_s	$2.2\,\mathrm{J\,m^{-1}\,s^{-1}\,K^{-1}}$	ρ_s	$1530\,\mathrm{kg\,m^{-3}}$	c_s	$2.28\times10^{6}\,\mathrm{J\,m^{-3}\,K^{-1}}$
k_p	$1.1\,\mathrm{J\,m^{-1}\,s^{-1}\,K^{-1}}$	ρ_p	$2230\,\mathrm{kg\,m^{-3}}$	c_p	$1.68\times10^{6}\,\mathrm{J\,m^{-3}\,K^{-1}}$
T_e	$-15.9\,^{\circ}\mathrm{C}$	Γ	$4.9\,^{\circ}\mathrm{C/wt\%}$	$\mathscr{L}_s$	$4.28\times10^{8}\,\mathrm{J\,m^{-3}}$
C_e	19.7 wt %				

TABLE 1. Physical property values used in the theoretical calculations.

where $G_1 = 1.9\times10^{-7}\,\mathrm{m\,s^{-1}\,K^{-1}}$ and $G_2 = 2.4\times10^{-8}\,\mathrm{m\,s^{-1}\,K^{-1}}$. With (4.8), equation (4.6) can be integrated numerically using the shooting method (Press *et al.* 1992).

The model was solved using parameters relevant to NH_4Cl–H_2O solutions, as listed in table 1. The results of the modelling are shown in figures 6 and 7. In figure 6 the predicted temperature profile is compared with the measured profile during an experiment using 25 wt % NH_4Cl pulled at $4\,\mu\mathrm{m\,s^{-1}}$. The theoretical curve reproduces fairly well the overall shape of the temperature profile, supporting our assumption that heat transfer in the melt occurs mainly by conduction. However, the measured temperature profile appears quite linear in the liquid region between $z = 2\,\mathrm{cm}$ and $z = 5\,\mathrm{cm}$. A theory capturing the effect of a double-diffusive layer ahead of the mush–liquid interface may yield closer agreement in that region. In figure 7 the model predictions are compared with the measured thickness of the mushy layer as a function of pulling speed V. The model shows good agreement at intermediate pulling speeds where there are no chimneys and partly into the regime where chimneys first appear. The model also predicts the disappearance of the mushy layer at high V (figure 4). However, when equiaxed crystallization occurred there was a significant reduction in the height of the mushy layer, as can be seen by the transition between stars or triangles and crosses in figure 7. This behaviour is not captured by the model. Also, the equations tend to overestimate the thickness of the mushy layer at lower speeds where chimneys are present. The disagreement between theory and experiment at low pulling speeds is probably due to the failure of two key assumptions in the model: that

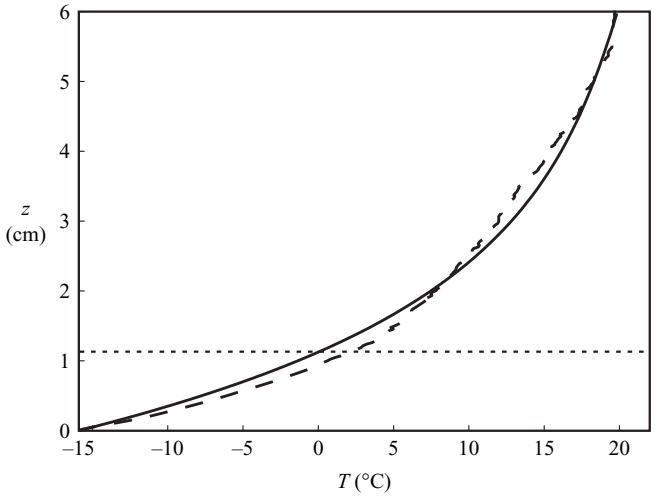

FIGURE 6. Measured (dashed) and predicted (solid) temperature profile during steady solidification of 25 wt% NH_4Cl at $4\,\mu m\,s^{-1}$. The horizontal dotted line shows the measured height of the mushy layer.

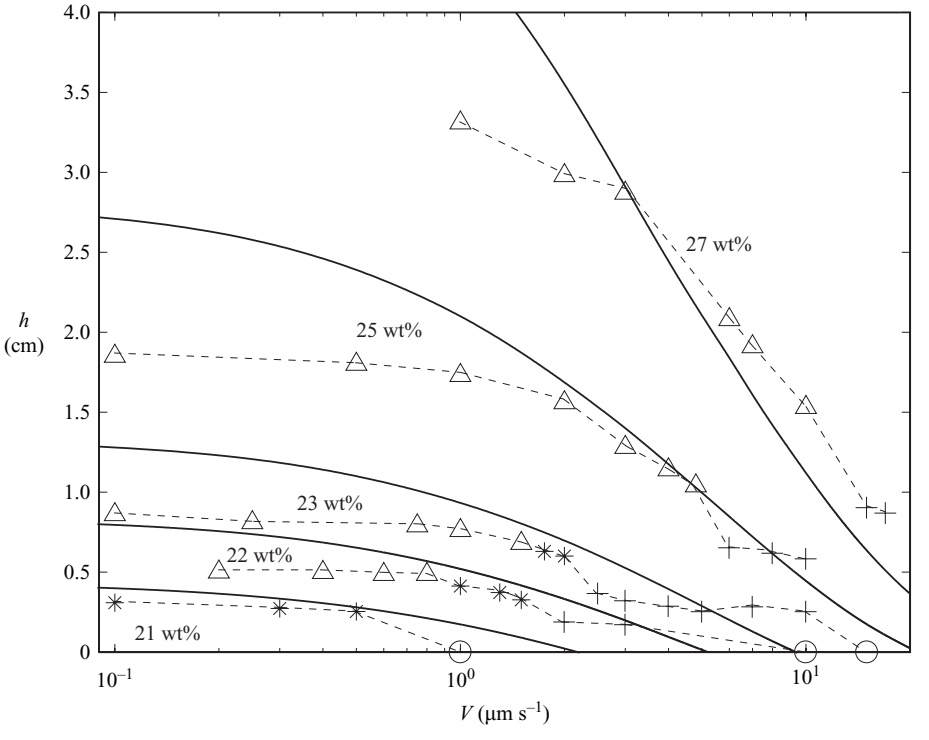

FIGURE 7. Measured (symbols) and predicted (solid curves) steady-state mushy layer heights h as functions of the pulling speed V. The symbols have the same meaning as in figure 4. The dashed lines join data points corresponding to the same initial concentration.

convection does not occur in the mushy layer and that no mass transfer occurs across the mush–melt interface. When chimneys are active the return flow brings warmer fluid from above down into the mushy layer, which inhibits its growth (Worster 2000).

5. Discussion

A key parameter characterizing the potential for convection in the mushy layer is the Rayleigh number (Worster 1997)

$$R_m = \frac{\Delta\rho g \Pi}{\mu V}, \tag{5.1}$$

where g is the acceleration due to gravity, Π is the permeability of the mushy layer, μ is the fluid viscosity, and $\Delta\rho$ is the density difference of the fluid across the mushy layer. For a linear dependence of ρ on concentration and temperature the density difference is $\Delta\rho = \beta[C(h) - C_e]$, where β is a constant incorporating the thermal and solutal expansion coefficients. Increasing the initial concentration C_0 has two effects: it increases $\Delta\rho$, which tends to increase R_m; it increases the solid fraction, which decreases Π and tends to decrease R_m. At the small values of $\mathscr{C} = (C_0 - C_e)/(C_s - C_0)$ characteristic of our experiments, the solid fraction and its variation with C_0 is small, and the Rayleigh number is dominated by the increase in $\Delta\rho$ as C_0 increases. Therefore, the system becomes more unstable as C_0 increases, as seen in figure 4 by the fact that the dashed curve separating triangles from stars slopes upwards. At much larger concentrations, we might expect the chimney to no-chimney transition to move to smaller values of V as C_0 increases but it seems from our experiments that the system may then be dominated by the equiaxed transition.

Convection in the melt is responsible for carrying supercooled liquid from the mush–solution interface out into the interior of the solution (Kerr *et al.* 1990), and may influence the onset of the nucleation and growth of secondary crystals (Kurz & Fisher 1989). There has been considerable discussion in the literature regarding the nature of the columnar–equiaxed transition that can occur in castings (Jackson *et al.* 1966; Flood & Hunt 1998). During dendritic solidification, crystal pieces (usually the detached side-arms of dendrites) can be continuously convected from the mushy layer into the melt (Hellawell, Liu & Lu 1997) or possibly nucleated above the mushy layer. The crystals grow in an equiaxed manner as they sediment downward and it is thought that they may eventually choke the mushy layer, causing it to collapse (Ni & Incropera 1995; Martorano, Beckermann & Gandin 2003). Convection in the melt could play an important role in determining the nature of the equiaxed transition (Kurz & Fisher 1989; Flood & Hunt 1998). The observations made in this paper may help to quantify some of these phenomena.

Near the boundaries between different solidification regimes exotic effects can occur. For example, movie 4 shows an experiment on 23 wt % NH_4Cl solidified at $1\,\mu m\,s^{-1}$, which is near to the chimney-extinction boundary. A 'breathing mode' occurs, in which the chimneys all periodically appear and disappear in phase. This behaviour may be related to an oscillatory convective instability (Anderson & Worster 1996; Guba & Worster 2006) and warrants further investigation.

6. Conclusion

Steady-state unidirectional solidification experiments were conducted on aqueous solutions of NH_4Cl in order to investigate the effects of convection on mushy layers. A small region in velocity–concentration parameter space was found within which uniform mushy layers can be grown. Outside this region defects occur either in the form of chimneys or the growth of secondary crystals. Quantifying the extent of the uniform region could have important implications for the design and manufacture of high-quality materials. A regime diagram is presented which illustrates the operating

conditions at which the various transitions occur. A simple mathematical model of the solidification process yielded good agreement with experimental measurements at velocities below the transition to secondary crystal growth, when chimneys were weak or absent.

We are grateful to M. A. Hallworth for technical assistance with the experiments. This research was funded by a grant from the Leverhulme Trust. The research of H.E.H. is partially supported by a Royal Society Wolfson Merit Research Award.

REFERENCES

Anderson, D. M. & Worster, M. G. 1996 A new oscillatory instability in a mushy layer during the solidification of binary alloys. *J. Fluid Mech.* **307**, 245–267.

Aussillous, P., Sederman, A. J., Gladden, L. F., Huppert, H. E. & Worster, M. G. 2006 Magnetic resonance imaging of structure and convection in solidifying mushy layers. *J. Fluid Mech.* **552**, 99–125.

Chen, C. F. 1995 Experimental study of convection in a mushy layer during directional solidification. *J. Fluid Mech.* **293**, 81–98.

Chen, F. & Chen, C. F. 1991 Experimental study of directional solidification of aqueous ammonium chloride solution. *J. Fluid Mech.* **227**, 567–586.

Chung, C.-A. & Worster, M. G. 2002 Steady state chimneys in a mushy layer. *J. Fluid Mech.* **455**, 387–411.

Copley, S. M., Giamei, A. F., Johnson, S. M. & Hornbecker, M. M. 1970 The origin of freckles in unidirectionally solidified castings. *Metall. Trans.* **1**, 2193–2204.

Davis, S. H. 2001 *Theory of Solidification*. Cambridge University Press.

Emms, P. & Fowler, A. C. 1994 Compositional convection and freckle formation in the solidification of binary alloys. *J. Fluid Mech.* **262**, 111–139.

Flood, S. C. & Hunt, J. D. 1998 Columnar to equiaxed transition. *ASM Handbook* **15**, 130–136.

Fowler, A. C. 1985 The formation of freckles in binary alloys. *IMA J. Appl. Maths* **35**, 159–174.

Guba, P. & Worster, M. G. 2006 Nonlinear oscillatory convection in mushy layers. *J. Fluid Mech.* **553**, 419–443.

Hellawell, A., Liu, S. & Lu S. Z. 1997 Dendrite fragmentation and the effects of fluid flow in castings. *JOM-J. Min. Met. Mat. Soc.* **49**, 18–20.

Huppert, H. E. 1990 The fluid mechanics of solidification. *J. Fluid Mech.* **212**, 209–240.

Huppert, H. E. & Hallworth, M. A. 1993 Solidification of NH4Cl and NH4Br from aqueous solutions contaminated with CuSO4: the extinction of chimneys. *J. Cryst. Growth* **130**, 495–506.

Huppert, H. E., Sparks, R. S. J., Wilson, J. R. & Hallworth, M. A. 1993 Cooling and crystallization at an inclined plate. *Earth Planet. Sci. Lett.* **79**, 319–328.

Huppert, H. E. & Worster, M. G. 1985 Dynamic solidification of a binary melt. *Nature* **314**, 703–707.

Jackson, K. A., Hunt, J. D., Uhlmann, D. R. & Seward, T. P. 1966 On the origin of the equiaxed zone in castings. *Trans. Metall. Soc. AIME* **236**, 149–158.

Kear, B. H. 1986 Advanced metals. *Sci. Am.* **255**, 159–167.

Kerr, R. C., Woods, A. W., Worster, M. G. & Huppert, H. E. 1990 Solidification of an alloy cooled from above. Part II: nonequilibrium interfacial kinetics. *J. Fluid Mech.* **217**, 331–348.

Kurz, W. & Fisher, D. J. 1989 *Fundamentals of Solidification*, 3rd Edn. Aedermannsdorf: Trans Tech. Publications.

Loper, D. E. & Roberts, P. H. 2001 Mush-chimney convection. *Stud. Appl. Maths* **106**, 187–227.

Martorano, M. A., Beckermann, C. & Gandin, Ch.-A. 2003 A solutal interaction mechanism for the columnar-to-equiaxed transition in alloy solidification. *Metall. Mater. Trans.* A **34**, 1657–1674.

McDonald, R. J. & Hunt, J. D. 1970 Convective fluid motion within the interdendritic liquid of a casting. *Metall. Trans.* **1**, 1787–1788.

Mullins, W. W. & Sekerka, R. F. 1964 Stability of a planar interface during solidification of a dilute binary alloy. *J. Appl. Phys.* **35**, 444–451.

Ni, J. & Incropera, F. P. 1995 Extension of the continuum model for transport phenomena occurring during metal alloy solidification – I. The conservation equations. *Intl J. Heat Mass Transfer* **38**, 1271–1296.

Peppin, S. S. L., Aussillous, P., Huppert, H. E. & Worster, M. G. 2007 Steady-state mushy layers: experiments and theory. *J. Fluid Mech.* **570**, 69–77.

Press, W. H., Teukolsky, S. A., Vetterling, W. T., & Flannery, B. P. 1992 *Numerical Recipes in C*, 2nd Edn. Cambridge University Press.

Roberts, P. H. & Loper, D. E. 1983 Towards a theory of the structure and evolution of a dendrite layer. In *Stellar and Planetary Magnetism* (ed. A. M. Soward), pp. 329–349. Gordon & Breach.

Schulze, T. M. & Worster, M. G. 1999 Weak convection, liquid inclusions and the formation of chimneys in mushy layers. *J. Fluid Mech.* **388**, 197–215.

Solomon, T. H. & Hartley, R. R. 1998 Measurements of the temperature field of mushy and liquid regions during solidification of aqueous ammonium chloride. *J. Fluid Mech.* **358**, 87–106.

Tait, S., Jahrling, K. & Jaupart, C. 1992 The planform of compositional convection and chimney formation in a mushy layer. *Nature* **359**, 406–408.

Wettlaufer, J. S., Worster, M. G. & Huppert H. E. 1997 Natural convection during solidification of an alloy from above with application to the evolution of sea ice. *J. Fluid Mech.* **344**, 291–316.

Worster, M. G. 1991 Natural convection in a mushy layer. *J. Fluid Mech.* **224**, 335–359.

Worster, M. G. 1992 Instabilities of the liquid and mushy regions during solidification of alloys. *J. Fluid Mech.* **237**, 649–669.

Worster, M. G. 1997 Convection in mushy layers. *J. Fluid Mech.* **29**, 91–122.

Worster, M. G. 2000 Solidification of fluids. In *Perspectives in Fluid Dynamics* (ed. G. K. Batchelor, H. K. Moffatt & M. G. Worster), pp. 393–446. Cambridge University Press.

Worster, M. G. & Kerr, R. C. 1994 The transient behaviour of alloys solidified from below prior to the formation of chimneys. *J. Fluid Mech.* **269**, 23–44.